



# Vegetation displacement issues and transition statistics in climate warming cycle<sup>1</sup>

L. Orlóci

*Department of Biology, University of Western Ontario, London, Canada N6A 5B7. E-mail: lorloci@uwo.ca, <http://www.vegetationdynamics.com>*

**Keywords:** Anthropogenic carbon; Denial machine; General trends; Late Quaternary vegetation; Transition metrics; Vostok temperature transformations; Warming-cooling rates.

**Abstract:** Scepticism largely deflated, and the denial machine's intent to mislead unmasked, climate warming owing to anthropogenic carbon emission is now seen by most as an ongoing process. When compared to the historic rates, the predicted warming rate and concomitant rates of biotic response should be considered simply colossal. This is the point about which the present paper gives insight based on numerical analyses. The Vostok temperature series, its different transforms, and palynological spectra from global sites are the basic data. These are marshalled in support of the paper's main proposition that the thermal effect on the vegetation depends not only on the rate of troposphere warming or cooling, but very much on the velocity of onset and length of duration. The main text begins with a definition of terms, followed by a short essay tracing how the conceptualisation of the climate warming paradigm evolved from initial scepticism to acceptance as a reality. The technical sections treat the conversion problem from Vostok inversion-layer temperature differences to global mean rates. It offers frequency distributions for historic warming/cooling rates, and explains the latitude dependence of the translation of the rates into local thermal flux. Presentation of examples of historic thermal events and the effect on the global vegetation close the main text. Statistical analyses are involved based on a novel methodology. The methods are concerned with formation migration rates, metrics of compositional transition velocity and acceleration, long-term variation in the representation of specific taxa in palynological spectra, taxon traits and taxon plasticity, and hotspots detection in compositional transitions. The palynological data are examined in synchrony with historic trends in the troposphere's Late Quaternary temperature history. Owing to the broad topical contents, the paper adapts a modular structure of presentation which requires the evaluation and interpretation of the results where they are presented. An overview is given at the end with emphasis on the general trends.

## Introduction

Displacement is our term for events of change in the geographic pattern of the vegetation. The papers focus is on the mechanistic aspects captured by displacement statistics associated with long-term global temperature oscillations. The transitions considered are global in scale, long-term, compositional, and functional. These are captured by individual taxon statistics and composite trajectory scalars extracted by complex analyses from palynological spectra. Figures 1 and 2 exemplify typical data sources available to us. Useful initial guidance to the methodology is found in Orlóci et al. (2002, 2006, Orlóci 2008).

An example of long-term (20 kyr) pattern displacements is presented in Fig. 1.4 of the Delcourt and Delcourt (1987) monograph. The figure, relevant for the vegetation history of Eastern North America, conjures impressions of a rather orderly, yet substantive space/time dynamics from Tundra to temperate deciduous forest, synchronic with long-term climate warming as the main trend that started about 16 kyr BP and lasted over millennia.

The process unfolds on different scales. The focus of the present paper is on the global scale, normally identified as the formation level. Much information is available for this level in the palynological spectra covering the Late Quaternary. It is quite clear from the available information that the assembly process has drawn on the same pool of species populations that re-emerge from refugia and expand their range with the onset of the favourable climate.

Assembly and disassembly as a perpetual process proceed at rates depending on the level of forcing. Important to the Late Quaternary process is that the rate of forcing by climate warming allowed time for the populations to absorb the thermal stress by ways of migration in locked step with the optimal climate. We show in this paper that no orderly process of that sort should be expected under even the most modest current predictions of global climate warming for the 21st Century. In fact, the 100 yr warming rate of 3.6°C, considered a below median prediction, may in fact turn out to have the potential of being very destructive because of the rapid onset well within the life span of many sessile organisms. Some of the predictions go beyond the 10<sup>0</sup> centennial climate

<sup>1</sup> This is written version of the lecture presented at Eötvös University, Budapest, in September 2007, extended and sections revised.

**Table 1.** Data sources by location and contact person. The number of taxa shown is the number listed in the original records. This is not necessarily the same number that we actually used, because of exclusions of ambiguous entries. Palynological data were downloaded from the Global Pollen Database (2007). Vegetation classification and precipitation data follow Küchler (1974, 1990) and Trewartha (1990). Potential evapotranspiration values are from Trewartha (2001). Legend to symbols: T – Tundra; TR – Tropical rainforest; LSC – Lowland shrub conifer; TA – Taiga; AT – Alpine tundra; TDF – Temperate deciduous forest; ARA – *Araucaria* forest; TG – Tropical grassland; G – other grassland; XF – Xerophytic forest; TH – Thorn shrub; EAS – *Eucalyptus*, *Acacia* shrub; EASC – EAS plus Conifer; MDSC – Montane desert shrub conifer; DS – Desert shrub. This table is taken from Orlóci et al. (2006)

Location and contact person	Latitude	Number of taxa	Period covered yr BP	Regional vegetation formation.
	Longitude Altitude (m)			Number of time steps.
1. Lagoa das Patas, Amazonas – P. E. Oliveira (Colinvaux et al. 1996)	00.16.00N	179	0 - 44569	TR
	66.41.00W	49		>200
	300			120-160
2. Joe Lake, Alaska – P. M. Anderson (1988)	66.46.00N	90	0 - 43804	T,TA
	157.13.00W	87		25-50
	183			<40
3. Camel Lake, Florida – E. C. Grimm (Watts et al. 1992)	30.16.00N	147	0 - 36658	LSC
	85.01.00W	116		100-150
	20			80-120
4. Hanging Lake, Yukon Territory – L. C. Cwynar (1982)	68.28N	89	0 - 41134	T
	138.23W	133		25-50
	500m			<40
5. Jack London Lake, Magadan Oblast, Russia – P. M. Anderson (Lozhkin et al. 1993)	62.10.00N	72	221 - 29876	AT,TA
	149.30.00E	60		25-50
	820			<40
6. Jackson Pond, Kentucky – G. R. Wilkins (Wilkins et al. 1991)	37.27.00N	71	0 - 20477	TDF
	85.43.00W	58		100-150
	212			80-120
7. Cambará, Rio Grande do Sul, Brazil – H. Behling (Behling et al. 2004)	29.03.09S	164	0 - 42784	ARA,G
	50.06.04W	190		150-200
	1046			80-120
8. Lake Patzcuaro, Michoacán de Ocampo, Mexico – W. A. Watts (Watts and Bradbury 1982)	19.35.00N	53	20 - 44100	XF
	101.35.00W	64		50-100
	2044			120-160
9. Rusaka Swamp, Burundi – R. Bonnefille (Bonnefille et al. 1995)	03.26.00S	179	796 - 11910 (46666)	TG,TH
	29.37.00E	141		50-150
	2070			120-160
10. Lynch's Crater, Queensland, Australia – A. P. Kershaw (1994)	17.22.00S	22	868 – 40000 (-192649)	EAS
	145.42.00E	44		50-150
	760	(234)		120-160
11. Harberton, Tierra del Fuego – V. Markgrah (no reference given).	54.53.00S	33	0 - 13360	DS
	67.10.00W	81		25-50
	20			80-120
12. Lake George, NSW – G. S. Hope (Singh and Geissler 1985)	35.05.00S	93	1 – 40000 (116711)	EASC
	149.25.00E	30		25-100
	673	(68)		80-120
13. Potato Lake, Arizona – R. S. Anderson (1993)	34.27.43N	77	1389 - 35271	MDSC
	111.20.43W	61		25-50
	2205			80-160
14. Hay Lake, Arizona – B. F. Jacobs (1985)	34.00.00N	44	106 - 44692	MDSC
	109.25.30W	46		25-50
	2780			80-160

warming rate. These rates, much higher than the ones that defined the current formation pattern of vegetation, are assumed to be sustained over the long term.

We put two questions to set limits on the otherwise very broad problem area:

1. Is troposphere warming real?
2. What to expect under the predicted warming rates in the way of dislocations and transitions?

We feel the first question can be handled in convincing detail based on evidence presented by others in selected benchmark publications. The question of displacements and transitions requires statistical analysis of archived long-term temperature and palynological data. The evidence in these is

left rather dormant by statisticians until recent development of an effective methodology (Orlóci et al. 2002, 2006, Orlóci 1994, 2008 and references therein). We build on an extended methodology and present novel results.

It is well established that the effect of climate warming depends on its rate of advance and its duration. We will examine these aspects in the main text after we addressed issues of reality, so that our conclusions to be drawn will be on all fours with what should we realistically expect.

### The reality of troposphere warming

It became known decades ago that anthropogenic CO<sub>2</sub> is increasing in the atmosphere and affecting the radiative heat balance and surface temperature of the Earth. Today the CO<sub>2</sub>

content in the atmosphere is 35% higher than before the Industrial Revolution in late 18th and early 19th centuries and it is higher than ever before in the last 500 k years. It became also known decades ago that CO<sub>2</sub> and other greenhouse gases, mainly methane and water vapour, are all on a relentless rise at rates equivalent in effect to doubling the atmos-

pheric CO<sub>2</sub> content of the atmosphere by 2070. A noted landmark publication presents the Mauna Kea graph CO<sub>2</sub> (Keeling et al. 1976, Thoning et al. 1989, Conway et al. 1994) that shows CO<sub>2</sub> rising at an ever increasing rate since 1958. The functional form of the rise is complex:

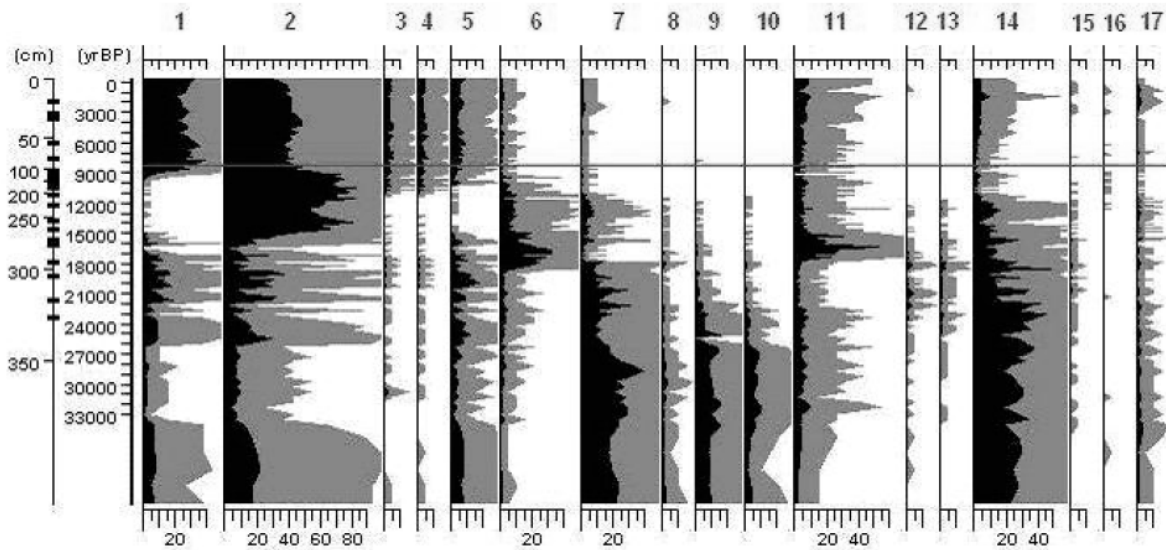


**Figure 1.** Cwynar's (1982) palynological spectrum from Hanging Lake, Yukon Territory. See Table 1 for site details. Short listed taxa after L.C. Cwynar: 1 *Alnus*, 2 *Betula*, 3 Ericaceae, 4 Ericales, 5 *Picea*, 6 *Salix*, 7 *Artemisia*, 8 Asteraceae-Asteroidae, 9 Brassicaceae, 10 Chenopodiaceae-Amaranthaceae, 11 Cyperaceae, 12 Fabaceae, 13 *Plantago canescens*, 14 Poaceae, 15 Rosaceae, 16 Other trees and shrubs, 17 Other herbs. Bottom scale: pollen counts %. Dark shading: original scale. Light shading: 5x exaggerated scale. Black markings on depth scale: dated horizons. Continuous line across table demarks a record set called *paleorelevé*. This is the virtual equivalent of the regional vegetation community 8200 years BP. Graph adapted from Orlóci et al. (2006) with permission. Data source: Global Pollen Database (2007).

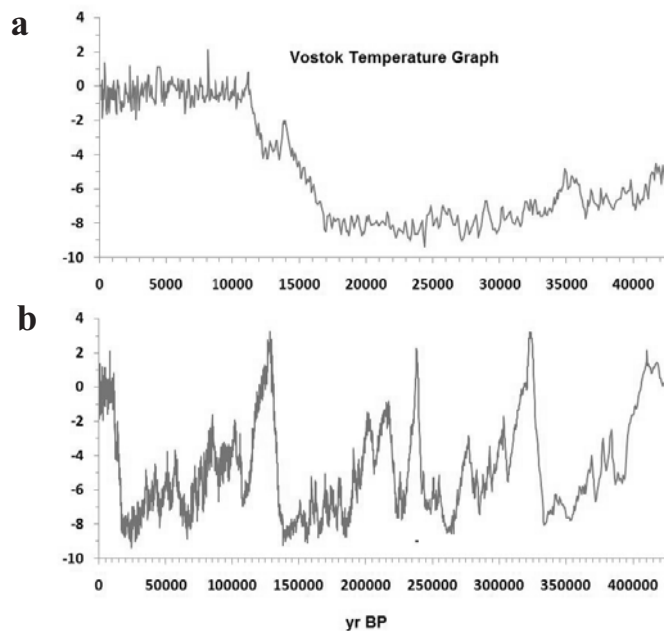


**Figure 2.** Oscillations of Vostok's inversion layer temperature, determined on the basis of deuterium found in the Anctartic ice. The graph's temperature scale expresses deviations from the current deuterium based inversion layer average temperature. The inversion layer is the site in the troposphere where precipitation originates. See Petit et al. (1999, 2001) for technical details on the ice core and determination of the ice's deuterium content. Data source: World Data Center for Paleoclimatology (2002).

$$y = 1082137.5 + 8859 X^{0.5} - 194450.384 \ln X$$

Symbol  $X$  stands for calendar year and  $y$  for CO<sub>2</sub> concentration in parts per million.  $y$  has to be multiplied by factor 743/350 to express the total atmospheric CO<sub>2</sub> in gigatons (Gt). Should present societal practices continue, fossil fuel burning will in all likelihood increase the CO<sub>2</sub> content of the atmosphere as follows:

Year	1990	2000	2010	2020	2050	2060	2090
CO <sub>2</sub> Gt	749	785	827	873	1041	1107	1332

The complete Mauna Kea record from 1958 to present is downloadable from the “trend” column in Tan’s (2008) data table. The 2008 web address for this is <ftp://ftp.cmdl.noaa.gov/ccg/co2/trends/co2\_mm\_mlo.txtis>.

A coupling of the empirical fact of the sharply rising CO<sub>2</sub> with the physical reality that this process upsets the radiative heat balance of the earth has raised the spectre of global climate warming. This necessarily leads to the next level of probing for evidence, represented by the global, predictive mathematical models. As of 1990, the most advanced one couples the ocean circulation with atmosphere circulation (Manabe et al. 1990). One of the outcomes is the prediction of 2.5° temperature rise in the troposphere by 2060. The prediction is linked to the “2 × CO<sub>2</sub>” scenario according to which the volume of greenhouse gases will have doubled by 2060 with effect compared to the doubling of the 1990 CO<sub>2</sub> content of the atmosphere. Projected for a 100 yr, the Manabe et al. (1990) warming rate would be 3.6°.

A significant step in the course of developments is J. Mason’s overview of models and climate warming basics in his 1990 Robens Coal Science Lecture at the Royal Institution of London. This is most remarkable for both perception, and in hindsight, for the accurate foresight. Mason made these points:

1. The radiative heat balance of the Earth has been tipped.
2. The amount of greenhouse gases held by the atmosphere [in 1990] is sufficient to make global climate warming a preordained event, and
3. the oceans’ thermal inertia, that made the climate warming signal too small to detect [in 1990] above the large natural climate variations, is destined to be overcome [speaking of about two decades up the road from 1990] at which point in time the oceans will start giving off the stored heat to the environment.

Mason (1990) clearly saw the need to head off the developing problem by implementation of appropriate steps and by developing appropriate long-term strategies, specifically,

“... to take all reasonable and practical steps to restrain or reduce energy consumption, and explore economically promising alternatives to fossil fuels.”

A U.K. reference, Mason considered necessary and realistic a governmental decision that would

“... restrict UK emissions of carbon dioxide by 2005 to current [1990] levels, and to reduce emission of CFCs in line with the Montreal Agreement.”

Speaking in the first person, Mason continued,

“In addition we should develop, without delay, adaptive strategies in agriculture, forestry, coastal defences, water supplies and so on, to make the economy less vulnerable to climate changes when they occur. It would appear that we have a breathing space of some 50 years [from 1990] but this may prove to optimistic; in any case it is none too long.”

While the trickle of reliable information that confirmed the danger of anthropogenically induced global warming as a hard reality by 1990, became a torrent during the 1990’s (Gore 1992, NSF 2001, IPCC 2001), underscoring further the importance of proper action to slow carbon dioxide emissions, a wait-and-see attitude became the dominant corporate and government policy. The ideological justification for this came from the sceptics (e.g., Lomborg 2001a,b) and from the industrial “denial machine”. Rebuttal of the sceptics’ arguments (e.g., Ege and Christiansen 2002) and successful unmasking of the denial machine were needed before policy changes could be expected at the highest levels. Publications by Kluger (2001), Lemonic (2001), Grady (2001), CBC (2006), Gore (2006), IPCC (2007) and Black (2007) prepared the ground. The signals of global warming, that were too small to detect, as J. Mason put it in 1990, are considered loud and clear in 2008. The massive melting of polar ice and glacial in the high mountains, the far too obvious transitions in the biota (Parmesan 2006), and not the least, the rising economic and social problems in countries trapped in regions under an already destabilised, marginal climate are élat examples.

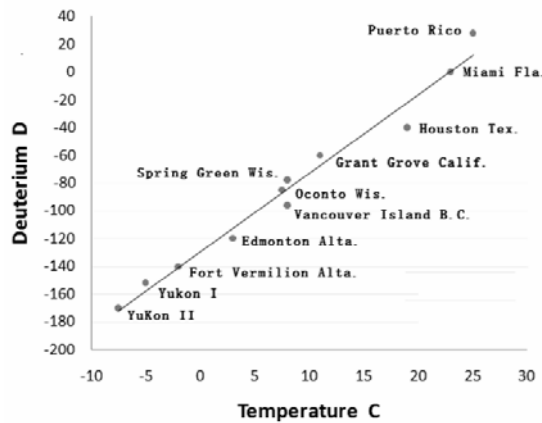
Climate warming is a fact, but the decision of exactly what steps to take has yet to be crafted. There are many options for the reduction of carbon dioxide in the atmosphere, but only industrial scale “carbon mining” may lead in time to substantial reductions. Relevant to this Sir Richard Branson’s offer of a \$25 m award:

“... for whoever can demonstrate to the judges’ satisfaction a commercially viable design which results in the removal of anthropogenic, atmospheric greenhouse gases so as to contribute materially to the stability of Earth’s climate.”

There are no takers of the Branson offer as yet.

While climate warming certainly has manageable aspects, if only society adopted an ecocentric mode of existence, as Thomas Berry (1988) describes it, in reality the prospects of society to adopt such an existence and thereby to manage the manageable aspects of global warming are receding into an ever more distant future.

The uncertainties facing us on our time scale are in sharp contrast with the certainties beyond that time scale in the millennia to come. We can say with certainty that in all likelihood the planetary mechanisms will continue functioning unchallenged, the concentration of land mass in the Northern Hemisphere will stay more or less unchanged, and the Milankovitch cycles (Milankovitch 1941) will do their work: the Earth’s climate will once more cool and a new glacial period will return.



$$D = 5.666T - 129.3; R^2 = 0.976$$

$$UL = 0.022T^2 + 5.289T - 120.8;$$

$$LL = -0.022T^2 + 6.039T - 137.8$$

**Figure 3.** Top: Deuterium content in the cellulose of tree rings (vertical axis) expressed in standard terms  $D = 1000(R_{\text{observed}} - R_{\text{ocean}}) / R_{\text{ocean}}$ . Symbols:  $R = {}^1H/{}^2H$ ,  ${}^1H$  amount of hydrogen and  ${}^2H$  amount of heavy hydrogen. Bottom: regression equations for  $D$  on temperature  $T$ , coefficient of determination  $R^2$ , upper (UL) and lower (LL) 95% confidence limits. Graph follows Gray and Se (1984) in Schweingruber (1996).

**Vostok temperature conversions**

The Vostok records (Petit et al. 1999, 2001) have fixed the historic thermal events in the inversion layer of the atmosphere at 78°28' S, 106°48' E as far back as 422.8 thousand years BP (Fig. 2). The records cover five interglacial periods and intermittent glaciations.

Conversion of temperature amplitudes to sites outside the Antarctic region is possible. Our factor for this is based on linear conversion rates applied in two steps:

1. Inversion layer temperature to surface temperature conversion:

$$K_1 = \frac{\text{Surface temp amplitude}}{\text{Inversion layer temp amplitude}} = \frac{12^\circ}{8^\circ} = 1.5$$

Petit et al (1999, 2000, 2001) are the relevant reference for specifics.

2. Vostok surface temperature to mean global temperature:

$$K_2 = \frac{\text{Current Global Mean Temperature}}{\text{Current Vostok Mean Temperature}} = \frac{289^\circ K}{218^\circ K} = 1.3$$

We note the current global mean temperature is taken to be 15 °C and the current Vostok mean surface temperature -55 °C. The product 1.5 × 1.3 amounts to 1.95, which we rounded to an even 2.

The following example should reveal that we deal with temperature differences. Let us suppose that we read -3.92° and 2.06° from the Vostok graph (Fig. 2) for time points 13 kyr BP and 5 kyr BP. This corresponds to a 100 yr inversion layer warming rate of 0.07475° and to a 100 yr surface warming rate in the global mean to 0.15°.

The Vostok temperature estimates are based on the deuterium (D) content in the ice core. Regarding the conversion,

the caption of Fig. 3 gives guidance (see Gray and Se 1984, Schweingruber 1996 and Petite et al. 1999, 2001). Using the regression equation from Fig. 3, the approximate local surface temperature can be estimated by  $T=(D+129.3)/5.7$  in °C. The D value is standardized. The deuterium source is usually dead organic matter, oceanic sediment, or ice.

**The unfolding of historic thermal events**

We are interested in warming and cooling episodes and the rates (temperature change in unit time) at which they unfolded. For comparability, we express the rates on a one hundred year basis. For example, if we read from the Vostok records 2.8° temperature increase over a 172 yr period then we take the 100 yr warming rate to be 1.6°.

To be logically comparable, not just the rates but the time step widths from which the rates are estimated should be the same. Time step width varies considerably within the Vostok series from 17 yr to almost 700 yr as seen in Fig. 4. It remains between 17 to 150 yr from present up to about 220 kyr BP. But beyond that point, it increases steeply and erratically. Considering these facts, we decided to exclude the 220 k yr BP to 4428 yr BP half of the series from the analysis when we examined the frequency distribution of the thermal change rates.

Equal time steps can be established after the fact only by interpolation, but this is at a cost to the resolving power of the data. The dilemma is, of course, how to strike a balance between improving comparability and keeping a high resolving power. If we opt for long time steps, we lower the amplitude of variation about the moving average with expected increasing loss of resolving power. If we opt for short time steps the spikes brought on by aberrant short term conditions will be emphasized. Ideally, the time steps should be sufficiently broad to filter out short-term aberrations while enhancing the appearance of robust trends.

**Table 2.** Frequency distribution of 100 yr cooling and warming rates in the Vostok series and its transforms. Upper class limits are shown for warming (+) and cooling (-) in header rows. Frequencies and relative frequencies are in body of the table. For example, 0.42 % of the 2645 rates larger than negative 2.5 but not larger than negative 2 indicates cooling at the average 100 yr rate of 2.25° inversion layer or 4.5° global mean surface temperature within the original (unadjusted) Vostok series. Frequencies are counted within the 0 to 220 kyr BP period. See the main text for explanation. Legend: ILR – upper class limits for inversion layer rates; GMSTR – upper class limits for global mean surface temperature; Vostok – original record set (A); Proxy 100 – Vostok record transformed to equal time steps 100 yr each (B); Proxy 600 - Vostok record set transformed to equal time steps 600 yr each (C).

A											
ILR	-4.5	-4	-3.5	-3	-2.5	-2	-1.5	-1	-0.5	0	0.5
GMSTR	-9	-8	-7	-6	-5	-4	-3	-2	-1	0	1
Vostok	1	2	1	3	5	11	19	62	263	1013	907
%	0.04	0.08	0.04	0.11	0.19	0.42	0.72	2.34	9.94	38.30	34.29
ILR		1	1.5	2	2.5	3	3.5	4	4.5	5	
GMSTR		2	3	4	5	6	7	8	9	10	TNS
Vostok		256	61	18	10	3	4	2	2	2	2645
%		9.68	2.31	0.68	0.38	0.11	0.15	0.08	0.08	0.08	100

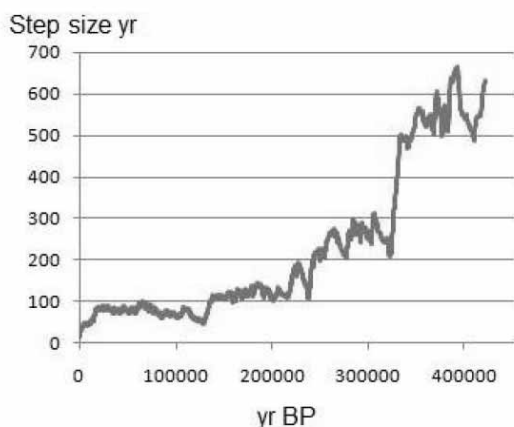
B									
ILR	-1.5	-1	-0.5	0	0.5	1	1.5	2	
GMSTR	-3	-2	-1	0	1	2	3	4	
Vostok 100	1	13	113	986	951	125	7	3	2199
%	0.05	0.59	5.14	44.84	43.25	5.68	0.32	0.14	100

C									
ILR	-1.5	-1	-0.5	0	0.5	1	1.5	2	
GMSTR	-3	-2	-1	0	1	2	3	4	
Vostok 600				352	352				704
%				50	50				100

With the forgoing thoughts in mind we examined the original Vostok series, keeping the original time steps. Then we created two proxy series by setting the equal time step width to 100 yr in one case and to 600 yr in the other case. The transformation involved is a time-step specific regression based interpolation.

We present the frequencies of warming/cooling rates for original, 100 yr and 600 yr time steps in Table 2. Typical instances of spiking over relatively short periods of time are



**Figure 4.** Time step differences in the Vostok series from present to 4228 kyr BP.

given in Table 3. Some interesting facts can be discovered from inspection of these tables:

1. The original time steps over emphasize the spikes. These tend to be short lived, albeit consequential at most only locally and mainly in marginal environments, unlike low-rate warming sustained over long periods. The latter were responsible for the rearrangement of the entire vegetation pattern in the northern hemisphere.

2. It is quite clear how far the short-term spikes stretch the tail of the distributions. While it is happening in a very symmetric manner, in all only 46 rates out of 2645 fall outside the negative 4° to positive 4° global mean surface temperature (GMST) limits. In total, 1920 of the 2645 cases occur within the negative 1° to positive 1° GMST limits. In general, the historic proportion of the 100 yr rates that are at least as large as 3.6°, the Manabe et al. (1990) prediction, is less than 1.5%. But basing such an estimate on the very variable original time steps is likely to be too liberal. Based on the proxy series, the proportion of the 100 yr rates that are at least as large as 3.6° is less than 0.14%. In the proxy series with 600 yr step size, none of the 704 stepwise rates is more extreme than negative 0.5° and positive 0.5°.

3. We emphasize that no extended period with warming rates sufficient to affect significantly the global vegetation pattern, such as the warming rates occurring in the 16974 to 11191 yr BP period, even came close to be as extreme as the median predictions today. For the full dimensions of the effect of thermal stress to be seen in local sites, the potentially

**Table 3.** Absolute and 100 yr warming/cooling rates in the Vostok series (0 to 220 kyr BP) and explanations based on the original untransformed Vostok series. Double the temperature difference and rate to obtain GMST estimates.

Period yr BP	Temperature °	Temperature difference °	Period yr	100 yr rate	Type	Cycle yr	Comment
16974-13938	-8.51, -2.06	6.45	3036	0.21	warming		Low-intensity long-term
13938-13539	-2.06, -4.02	1.96	399	0.49	cooling	3435	warming trends that shaped the modern high-level global vegetation pattern.
13539-12385	-4.02, -3.96	0.10	1154	0.01	cooling		
12385-11191	-3.96, 0.81	4.77	1194	0.40	warming	2348	
8276-8135	-0.78, 2.06	2.84	141	2.01	warming		Short-term high-rate
8135-7994	2.06, -0.54	2.60	141	1.84	cooling	282	spikes, that probably accelerated early
4690-4509	-0.88, 1.13	1.92	181	1.06	warming		developments in agriculture
4339-4202	1.13, -1.00	2.13	137	1.55	cooling	488	and also forced catastrophic draughts in marginal environments.
2331-2291	-0.98, 1.16	2.14	40	5.35	warming		
2291-2212	1.16, -0.73	1.89	79	2.39	cooling	119	
552-397	-1.61, 1.33	2.94	155	1.90	warming		
397-234	1.33, -1.84	3.17	163	1.94	cooling	328	
234-190	-1.84, 0.23	2.07	44	4.70	warming	44	

substantial local thermal flux rates have to be taken into account (Orlóci 1994).

### Local thermal flux rates

It is a well know fact that latitude can affect the rate at which any rise in the global average temperature translates itself into local temperature rise. For example, moving North on the Delcourt and Delcourt (1987) transect in Eastern North America, the impact of global warming should be felt at an increased rate. Orlóci (1994) used a simple but effective method, based on vegetation formations as geographic markers, to estimate local thermal flux rates (*LTFR*) from current surface temperature, current global mean temperature, and historic global mean temperature. His equation is

$$LTFR = \left| \frac{CTHN - CTCN}{GTH - GTC} \right|$$

In this, *LTFR* is the rate at which one degree rise in the global mean surface temperature will materialise as a local temperature rise. Symbols: *CTHN* - current temperature at the more southern historic northern limit of the marker vegetation formation; *CTCN* - current temperature at current northern limit of marker vegetation formation; *GTH* - historic global mean surface temperature at the time when the formation reached a more southern, northern limit, from where it migrated to its present, northern limit; *GTC*: current global mean temperature. Table 4 contains examples from Eastern North America roughly along longitude 85° W. We also include some altitudinal cases from Mauna Kea on the Big Island of Hawaii. Marker boundary shifts are read from figure 1.4 of Delcourt and Delcourt (1987) for the North American sites and from Cruikshank (1986) on Mauna Kea.

Two things are quite obvious:

1. The thermal flux rate is functionally related to latitude ( $LTFR = -1.276 + 0.065X$  and  $R^2 = 0.99$ ). Only the North American sites are included in the calculations.

2. Moving North, the thermal flux rate becomes increasingly extreme. At those rates even a modest 3.6° increase in the global average temperature would cause a catastrophic rise in the local temperature, far beyond the temperature regimes in the distribution area of the key Boreal Forest, Taiga and Tundra plants.

The premises of estimation are straight forward and the method can be applied at very little cost to the user. An added advantage compared to the mega-models, is that the estimated *LTFR* values have local relevance.

### Past and anticipated climate warming effects

It can be concluded from what has already been presented above that a 3.6 °C 100 yr warming rate, a very conservative value among recent predictions, is already in the category of the historically very low frequency sustained warming events. Climate warming occurred at that rate about 3 times over the 219.9 kyr period (see Table 2, 100 yr step size). In the following sections we examine examples to illuminate further what to expect based on past effects under historic warming rates that caused taxa, and metaphorically speaking, entire vegetation zones to migrate long distances.

Specifically, we examine certain salient characteristics of vegetation dynamics whose traces are recognisable in the palynological spectra. Formation expansion rate is one of these for which the time/space pattern dynamics mapped by Delcourt and Delcourt (1987, figure 1.4, page 20) in Eastern North America is an example. The long-term oscillations of characteristic community metrics is another property that we discuss, recapitulating results presented in earlier papers by us (Orlóci et al. 2002, 2006, Orlóci 2008). The long-term oscillation of taxon frequencies is yet another topic we exam-

**Table 4.** Local thermal flux rate estimates based on Orlóci's (1994) method. The vegetation records for Mauna Kea follow Krajina (1963). Data in rows 3,4 are from Walter et al. (1975), except in the last two cells, which are from Krajina (1963). It is to be noted that thermal flux rates are specific to the sites where they are determined. Abbreviations: AMP – annual mean precipitation; AMT – annual mean temperature; LTFR – local thermal flux rate; TR - local temperature rise; EAMT - expected annual mean temperature under the Manabe et al. (1990) 3.6 °C global warming scenario on a 100 year basis (2.5 °C temperature rise in 70 years).

Vegetation	Arctic Tundra	Boreal	Mixed Conifer- Northern Hardwood	Cool Temperate Deciduous	Warm Temperate Evergreen	Tropical Alpine (3,300m)	Tropical Subalpine (2,000m)
1 Climatic station	Port Harrison, Qu.	Timmins, Ontario	Stratford, Ontario	Nashville, Tennessee	Mobil, Alabama*	Mauna Kea, Hawaii	
2 N.lat. X	58°26'	48° 31'	43° 22'	36° 10'	31° 42'	19° 49'	19° 49'
3 AMP mm	372	711	773	1,144	1,439	510	1020
4 AMT °C	-7.5	1.3	8.3	15.6	19.8	0	4.4
5 LTFR	2.53	1.92	1.5	1.1	0.8**	0.92	0.92
6 TR	9.1	6.9	5.5	3.9	3.6	3.32	3.32
7 EAMT	1.6	8.2	13.8	19.5	23.4	3.32	7.72

\* Not climate related limit. \*\* Extrapolation according to regression equation in the text.

ine. Our taxa are pollen types found in the palynological spectra. We also consider metrics that capture the communality and specificity traits of the palynomorphs, interpretable in terms of plasticity and community assembly tendencies. Our last example is devoted to a discussion of compositional transition hotspots.

#### Formation expansion rate in warming cycle

Under sustained but moderate warming or cooling climates, entire vegetation zones may be dislodged and their component species forced to migrate and reassemble in new geographic locations. Delcourt and Delcourt (1987, figure 1.4, page 20) fixed the time/space dynamics of such a process over 20 kyr in Eastern North America. Focusing on the Eastern Deciduous Forest (D in Fig. 5), we observe that this formation did not exist until about 13 kyr BP, when it began to assemble from species migrating out of refugia. The following statistics are revealing:

1. Formation begins to assemble 13 kyr BP on latitude 33° N. For this time point, we read -4.25° from Fig. 2.

2. By 5 kyr BP, the formation expands 10° north. For this time point, we read 0.13° from Fig. 2. The difference in *GMST* terms is 8.76 which corresponds to an average 100 yr warming rate of 0.11° over the 8 kyr period. The corresponding centenary dislocation rate of the northern limit of the formation is  $10/80=0.13^\circ \text{LN}$ .

3. At the predicted current 100 yr climate warming rate of 3.6 °C, which materialises as a  $3.6 \times 1.5 = 5.4^\circ$  100 yr local warming rate at the northern limit of the formation, northern boundary dislocation northward should occur at the 100 yr rate of  $(5.4^\circ \times 0.13^\circ)/0.11^\circ = 6.38^\circ \text{LN}$ . This is about 50 times the historic rate. Few plant species of the Eastern Deciduous Forest would be capable of migrating northward at that rate,

and the few that could, would quickly run out of available terrestrial geography.

#### Long-term oscillations of characteristic community metrics

One of the metrics is compositional transitions velocity *V*. It is defined as the amount of compositional change in unit

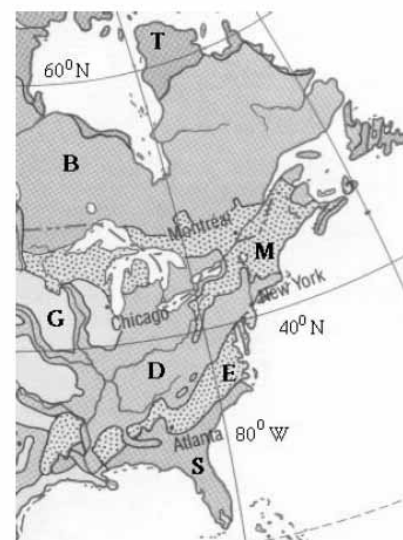


**Figure 5.** Vegetation map of Eastern North America after Küchler (1988 with revisions). Legend to formations: T – Tundra; B – Boreal Forest; M – Mixed Conifer-Northern Hardwood Forest; D – Cool-Temperate Deciduous Forest; G – Grassland; E – Warm-Temperate South-Eastern Evergreen Forest; S – Sub-tropical Forests. See Braun (1950) for detailed description of D, the target vegetation formation of this section of the paper.

**Table 5.** Regression estimates for the correlation of Vostok temperatures and compositional transition velocity in paleospectra from 14 global sites. Refer to Petite et al. (1999) and Fig. 2 on Vostok, to Fig. 6 and Orlóci et al. (2002, 2006, Orlóci 2008) for the regression estimation used, and to the Global Pollen Database (2007) for details on data sources. Symbols:  $V$  – compositional transition velocity,  $T$  – Vostok temperature,  $r(V,T)$  – a multiscale regression estimate of the correlation,  $R^2$  – coefficient of determination in regression,  $F^+$  and  $F^-$  – analytically derived sign frequencies of the correlation,  $Thi$  – Thornthwaite index (precipitation per potential evapotranspiration), CRVF – current regional vegetation formation,  $TU$  – Tundra;  $TR$  – Tropical rainforest;  $LSC$  – Lowland shrub conifer;  $TA$  – Taiga;  $AT$  – Alpine tundra;  $TDF$  – Temperate deciduous forest;  $ARA$  – Araucaria forest;  $TG$  – Tropical grassland;  $G$  – other grassland;  $XF$  – Xerophytic forest;  $TH$  – Thorn shrub;  $EAS$  – Eucalyptus, acacia shrub;  $EASC$  –  $EAS$  plus Conifer;  $MDSC$  – Montane desert shrub conifer;  $DS$  – Desert shrub. Note the declining values in the  $\phi^+$  column and the increasing values in the  $\phi^-$  column with declining values of the Thornthwaite index ( $Thi$ ) in the 0 to 50 yr BP and the 10 to 50 yr BP intervals. Their numerical correlations are given in Table 6. Table reproduced from Orlóci et al. (2006) with change.

Statistics		$\rho(V,T)$	$\rho(V,T)$	$\rho(V,T)$	$\phi^+$	$\phi^-$	$\phi^+$	$\phi^-$	$\phi^+$	$\phi^-$	$Thi$	CRVF
#	Period kyr	0-50	0-10	10-50	0-50	0-50	0-10	0-10	10-50	10-50		
1	Lagoa das Patas 00.16N 6.41W	0.12	-0.2	0.46	81	16.3	47.6	39	86.4	10.9	1.4	TR
2	Joel Lake 66.46N 157.13W	0.35	-0.01	0.83	80.9	16.8	53.6	32.6	94.61	4.95	1.9	TU
3	Camel Lake 30.16N 85.01W	0.31	0.39	0.6	75.8	20.7	99	1	66.3	31.2	1.3	LSC
4	Hanging Lake 68.28N 138.23W	0.63	-0.5	0.83	68.7	30.2	2.23	94.6	65.7	33.3	1.9	TA
5	Jack London L. 62.10N 149.30E	0.11	-0.5	0.55	65.1	29.2	25.8	64.2	85.1	3.58	1.9	AT TA
6	Jackson Pond 37.27N 85.43W	0.3	0.4	0.61	57.3	38.4	69.8	28.1	76.7	20.7	1.3	TDF
7	Cambará 29.03S 50.06W	0.53	0.03	0.29	56.6	32.8	55.4	31.4	52.5	35.3	1.8	ARA G
8	Rusaka Swamp 3.25S 29.37E	0.23	-0.04	0.76	46.8	40	33.2	65.6	84.7	13.2	0.7	TG TH
9	Lynch's Crater* 17.22S 145.42E	-0.7	0.26	-0.2	42.6	55.1	76.3	14	39.2	49.9	0.7	EAS
10	Tierra del Fuego 54.53S 67.10W	-0.3	-0.1	0.47	33.6	63.7	26.2	67.4	73.2	23.6	0.4	DS
11	Lake George* 35.05S 149.25E	-0.5	0.55	-0.2	15.1	84.3	78.4	20.8	32	66.4	0.6	EASC
12	Potato Lake 37.27N 111.20W	-0.3	-0.2	-0.2	11.2	84.9	38.1	51.2	38.1	51.2	0.3	MDSC
13	Hay Lake 34.00N 109.25W	-0.2	-0.6	0.61	4.74	93.9	3.28	96.7	16.2	80.5	0.3	MDSC

\*Last 50 kyr

**Table 6.** Correlation of the regional  $r(V,T)$  values and sign frequencies ( $\phi^+$ ,  $\phi^-$ ) with current estimates of the Thornthwaite index ( $Thi$ ) as given in Table 5. Large  $\rho(\phi^+, Thi)$  indicates strong linkage of climate warming and accelerated compositional transitions in the humid zones. This also indicates increased, warming related, compositional instability. Nominally large  $\rho(\phi^-, Thi)$  indicates that the effect is reversed in the arid zones where warming tends to slow the transition process.

Period	$\rho(V,T) \times Thi$	$\rho(\phi^+, Thi)$	$\rho(\phi^-, Thi)$	Regularities recognized
Total period 0 – 50 kyr BP	0.775	0.851	-0.844	Se Caption
Pre-Holocene 10-50 kyr BP	0.537	0.604	-0.626	50 kyr regularity retained.
Holocene 0 – 10 kyr BP	-0.136	0.031	-0.103	Pre-Holocene pattern collapses.

time (Orlóci et al. 2002, 2006, Orlóci 2008). The first derivative of  $V$  is the transition process acceleration  $A$ , which is the change in velocity per unit time. We examined the long-term oscillations of  $V$  and  $A$  in 14 paleospectra (Fig. 6, Table 5) and measured the synchronicity with the Vostok temperature oscillation (Fig. 2), using specialized techniques (Orlóci et al. 2002, 2006, Orlóci 2008). A typical case, taken from Cwynar (1982) is featured in Fig. 6. Other cases are identified in Table 1 and detailed results in Table 5. Notwithstanding the extreme nature of oscillations, the synchronicity with temperature oscillations is clear: dominantly positive in sites of the humid biomes and negative in sites of the arid biomes. This suggests the definite biome dependence of warming effects and concomitant levels of compositional destabilization. By destabilization we mean the tendency for rapid change.

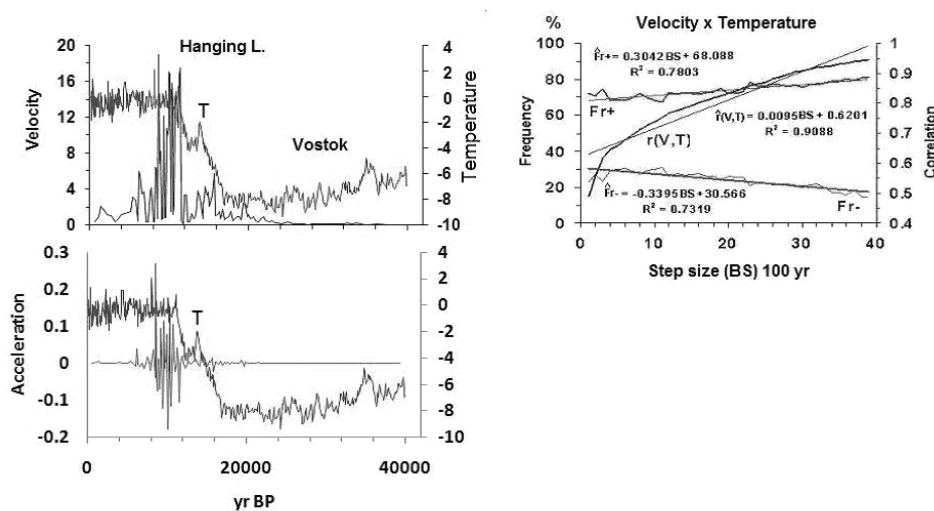
#### Long-term taxon frequency oscillations

Taxa in this case are the pollen types or palynomorphs. Fig. 7 presents characteristic graphs. The oscillations are relative to random expectation, which is a frequency value to be expected where and when pollen type dispersion is con-

trolled by a purely random process. The method of construction is described by Orlóci et al. (2002, 2006), Orlóci (2008).

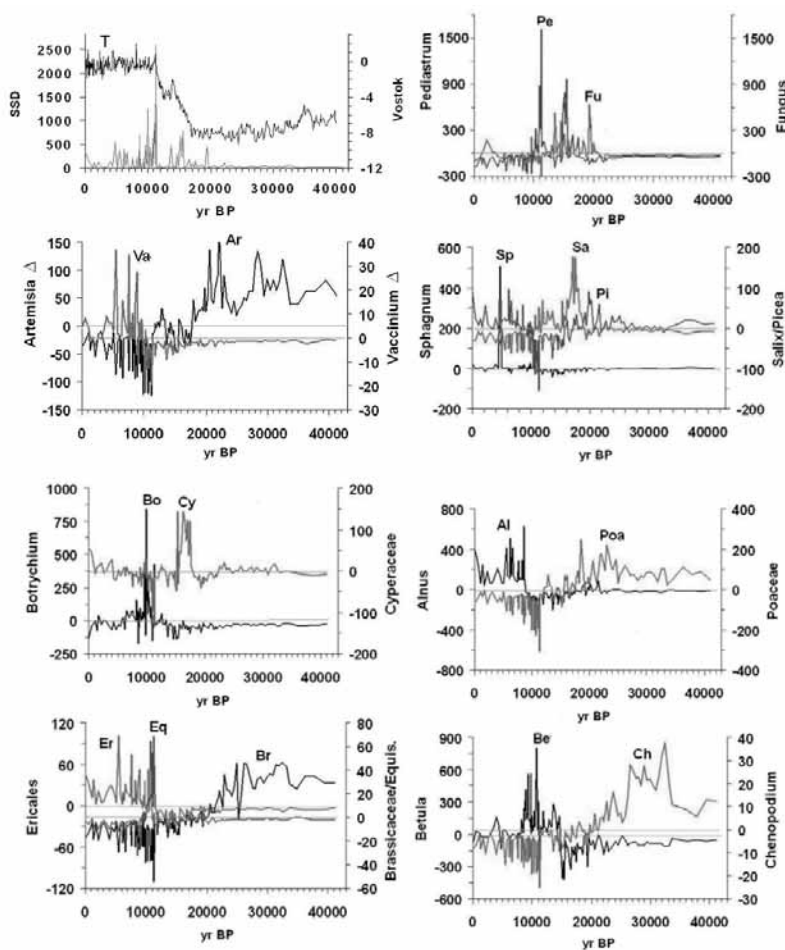
The deviation graphs highlight the long-march of palynomorphs through time, or metaphorically speaking, through successive life zones (cold step, tundra, and taiga) over the 40 kyr history of the Hanging Lake sediments. Dry step taxa (Poaceae, *Artemisia*, Brassicaceae, *Chenopodiaceae/Amaranthaceae*) dominate the region's uplands until about 19 kyr BP, the lichen-rich tundra (*Pediastrum* alga + Fungi spore types) thereafter until about 11 kyr BP, to be succeeded by the Taiga under increased precipitation. The collection of palynomorphs characteristic for the Taiga include *Betula*, *Alnus incana*, *Botrychium*, *Sphagnum*, *Picea*, Ericales, *Equisetum*, and *Vaccinium*.

The graphs show changes in deviations ( $\Delta$ ) and sums of squared deviations ( $SSD$ ). The  $SSD$  graph is the sum of the squared  $\Delta$  graphs. The cumulative effect of climate warming is unmistakable in both types of graphs (first plate, Fig. 7). As far as the long-past is concerned, well within the cooling cycle, the early, rather flat temperature graph coincides with uniformly low amplitude portions of the  $\Delta$  graphs. Climate



**Figure 6.** Left column: oscillograms for compositional transition velocity, compositional transition acceleration, and Vostok temperature. Measurement units are arbitrary. Velocity is defined as the amount of compositional transition per unit time. Acceleration is the rate of change in velocity. Right column: graphical representation of correlation analysis adopted from Orlóci et al. (2002, 2006). Three irregular lines are shown and three straight lines. The irregular line labelled  $r(V,T)$  captures the synchronicity of velocity and temperature computed over the entire period length (422.8 kyr) at different step sizes  $BS$ . The corresponding straight line is the best fitting regression line  $r(V,T) = 0.0095BS + 0.6201$ . The irregular line labelled  $Fr^+$  represents the frequency of positive  $r(V,T)$  values within a very large number of randomly chosen substrings fitted within the total period length. The corresponding regression line is  $Fr^+ = 0.3942BS + 68.088$ . The irregular line  $Fr^-$  represents the frequencies of the negative  $r(V,T)$  values for which the regression equation is  $Fr^- = -0.3395BS + 30.566$ .  $R^2$  is the coefficient of determination for regression. Graphs are viewable in colour at Web address <http://www.vegetationdynamics.com> link [VDIFigures.pdf](http://www.vegetationdynamics.com).

**Figure 7.** Long-term oscillations of leading taxa (palynomorphs) in the Hanging Lake spectrum (Table 3). Graph follows Orlóci et al. (2002, 2006), Orlóci (2008). Horizontal axis: years before present. Vertical axis: Vostok temperature differences ( $T$  in first plate) following Petit et al. (1999, 2001), sums of squared deviations ( $SSD$ ) and deviations from random expectation ( $\Delta$ ). Random expectation is the hypothetical state under which compositional transitions are ruled entirely by chance. Deviations above or below random expectation (the zero line) indicate over or under-representation of the specific taxa in relative terms. The following percentages indicate proportions of the total sum of squared deviation ( $SSD$ ) accounted for by the individual taxa in the total sample of 89 taxa: *Betula* 19.1%, Fungus (ascospores component in lichen) 8.5%; *Artemisia* 2.2%; *Sphagnum* 1.5%; *Salix* 0.9%; *Chenopodiaceae/Amaranthaceae* 0.1%; *Vaccinium* 0.01%. Graphs are viewable in colour at Web address <http://www.vegetationdynamics.com> link [VDIFigures.pdf](http://www.vegetationdynamics.com).



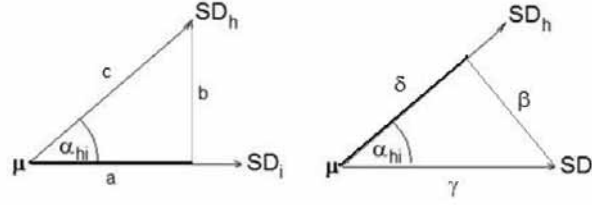


**Figure 8.** Isolation of the communality ( $a, \delta$ ) and specificity ( $b, \beta$ ) components of variation for taxon  $h$  with regard to taxon  $i$  and for taxon  $i$  with regard to taxon  $h$ . Definition of relevant quantities:  $SD_h = \sqrt{S_{hh}}$  – standard deviation, taxon  $h$ ;  $SD_i = \sqrt{S_{ii}}$  – standard deviation, taxon  $i$ ;  $S_{hh} = a^2 + b^2 = c^2$  – variance, taxon  $h$ ;  $S_{ii} = \delta^2 + \beta^2 = \gamma^2$  – variance, taxon  $i$ ;  $S_{hhc|j} = c^2 \cos \alpha_{hi} = a^2$  – portion of the variance of taxon  $h$  that can be accounted for by the correlation with taxon  $i$ ;  $S_{hhs|j} = c^2 \sin \alpha_{hi} = b^2$  – portion of the variance of taxon  $h$  that cannot be accounted for by co-variation with taxon  $i$ ;  $S_{iic|h} = \gamma^2 \cos \alpha_{hi} = \delta^2$  – portion of the variance of taxon  $i$  that can be accounted for by the correlation with taxon  $h$ ;  $S_{iis|h} = \gamma^2 \sin \alpha_{hi} = \beta^2$  – portion of the variance of taxon  $i$  that cannot be accounted for by co-variation with taxon  $h$ ;  $r_{hi} = \cos \alpha_{hi} = S_{hi} / (S_{hh}S_{ii})^{1/2}$  – the correlation coefficient of taxon  $h$  and taxon  $i$ ;  $S_{hh} = S_{hhc|j} + S_{hhs|j}$ ;  $S_{ii} = S_{iic|h} + S_{iis|h}$ . Note: a  $90^\circ$  alpha angle implies independence, such as  $a=0$  and  $b=c$  or  $\delta=0$  and  $\beta=\gamma$ . See further technical details in the main text.

warming brings out the deviation peaks. A typical case is the SSD peak around 11 kyr BP that comes at the end of a long period of surface warming at a 100 yr rate of about  $0.8^\circ\text{C}$  (a warming rate less than one fourth of the Manabe prediction).

#### Taxon traits and assembly metrics

Palynological spectra hold information about the long-term contribution of taxa to community dynamics. The contribution may have many aspects of which those that relate to community assembly is readily measured in terms of a taxon's dual traits called *communality* and *specificity* (Orlóci 1975, 1978 pp. 31 et seq.) The communality metric  $R^2_{h|}$  is defined as the squared multiple correlation coefficient. Subscript  $h$  refers to a taxon. The other is the taxon's specificity metric, the one complement of the squared multiple correlation,  $1-R^2_{h|}$ . We revisit Orłóci (1978) for salient points of derivation guided by the diagram in Fig. 8. Important note: for meaningful results in the manipulations below, the distribution of individual taxa chosen should span the entire depth of the spectrum, and the spectrum should be constructed from many samples (data points).

Based on the level of communality or specificity, taxa are categorised by trait as *team-players* (A) and *individualists* (B). Most taxa fit in between the two extremes with one of the traits being dominant. We will classify taxa as A or B depending on the dominant trait. Our classification rule for trait A or B is the greater of  $R^2_{h|}$ , or  $1-R^2_{h|}$ . We call  $R^2_{h|}$  the squared multiple correlation of  $h$  with the other taxa and give it functional form as  $R^2_{h|} = S_{hhc}/S_{hh}$ . In this,  $S_{hhc}$  is the communality variance of taxon  $h$  with the other taxa and  $S_{hh}$  is the total variance of taxon  $h$ . Orłóci (1975, 1978, Orłóci and Orłóci 1995) describe two methods to compute values for the right hand terms in:  $S_{hh} = S_{hhc} + S_{hhs}$ .

1. The first method requires a non-singular variance/covariance matrix  $\mathcal{S}$  of taxa. That is, the inverse of matrix  $\mathcal{S}$  must exist. This requires a spectrum not saturated with zeros. In other words, the taxa must span the spectrum. To establish this condition, the taxa with low constancy have to be re-

moved. If in fact the inverse of  $\mathcal{S}$  found to exist, then the partition  $S_{hh} = S_{hhc} + S_{hhs}$  is accomplishable simply by taking  $S_{hhs} = 1/S^1_{hh}$ , in which  $S^1_{hh}$  is the  $h, h$  diagonal element in the inverse of matrix  $\mathcal{S}$ . Based on the partition, we have the multiple correlation of taxon  $h$ :

$$R_{h|} = \sqrt{\frac{S_{hhc}}{S_{hh}}}.$$

$R^2_{h|}$  is the level of relative redundancy (co-variation) of taxon  $h$  with respect to the other taxa involved in the computations.

2. An alternative method for computing the partition  $S_{hh} = S_{hhc} + S_{hhs}$  does not require matrix inversion. The algorithm is recursive through steps involving computation of  $S_{hhc|j}$  partial communality values from the stepwise residuals of  $\mathcal{S}$ . The number of partial communalities is one less than the order of  $\mathcal{S}$ . The step-wise partial communalities are summed to obtain the  $S_{hhc}$  value. Here in brief, what is developed at length in Orłóci (1975, 1978, pp. 18 et seq.), the recursive calculations go like this assuming that the rows in the basic  $p \times n$  data matrix  $\mathbf{X}$  are taxa:

1. Compute  $S_{hk(0)} = \sum_{j=1}^n x_{hj}x_{kj}$  in which  $x_{hj} = X_{hj} - m_h$

$$\text{and } m_h = \frac{1}{n} \sum_{j=1}^n X_{hj}.$$

2. Compute the communality of taxon  $h$  with taxon  $i$

$$S_{hhc(0)} = \frac{S_{hi}}{\sqrt{S_{hh}}} = \delta_{hh|i},$$

and specificity  $S_{hhs(0)} = S_{hh} - \delta^2_{hh|i}$ .

3. Compute the first residual of  $\mathcal{S}$ :

$$S_{hk(1)} = S_{hk} - \frac{S_{hi}}{\sqrt{S_{ii}}} \frac{S_{ki}}{\sqrt{S_{kk}}}.$$

**Table 7.** The duality of communality and individualistic traits in the taxa taken from the Hanging Lake spectrum in the Canadian Arctic and from the Cambará spectrum on the temperate Rio Grande do Sul Highlands in Brazil. Table 1 contains the site and data specifications. The 10 most frequency taxa are selected for analysis. The number of available taxa is 89 in Hanging Lake and 164 in Cambará. See reasoning in the main text. Symbols: *FR* – taxon frequency, i.e., the number of the sampled sediment horizons (data points) in which the taxon occurs. The total number of data points is 133 in the Hanging Lake spectrum and 190 in the Cambará spectrum;  $R^2_{h|}$  – the multiple correlation coefficient of taxon *h* in the spectrum measured on the 0 to 1 scale; this is an expression of the strength of trait communality; - a measure of the strength of trait specificity. Note: the taxa csn shift dominant traits within the different historic periods (0-10 kyr BP, 11-20 kyr BP, 20-41 kyr BP).

Hanging Lake, Yukon							
# Taxa	FR	0 to 10 kyr BP		11 to 20 kyr BP		20 to 41 kyr BP	
		$R^2_{h }$	$1-R^2_{h }$	$R^2_{h }$	$1-R^2_{h }$	$R^2_{h }$	$1-R^2_{h }$
1 Betula	133	<b>0.81</b>	0.19	<b>0.93</b>	0.07	0.18	<b>0.82</b>
2 Poaceae	133	0.34	<b>0.66</b>	<b>0.71</b>	0.29	0.10	<b>0.90</b>
3 Salix	132	<b>0.53</b>	0.47	<b>0.59</b>	0.41	<b>0.53</b>	0.47
4 Artemisia	132	<b>0.86</b>	0.14	<b>0.92</b>	0.08	0.21	<b>0.79</b>
5 Cyperaceae	132	0.44	<b>0.56</b>	0.34	<b>0.66</b>	0.04	<b>0.96</b>
6 Picea	129	<b>0.69</b>	0.31	<b>0.59</b>	0.41	0.17	<b>0.83</b>
7 Alnus viridis	123	0.40	<b>0.6</b>	<b>0.81</b>	0.19	0.26	<b>0.74</b>
8 Sphagnum	121	<b>0.53</b>	0.47	<b>0.63</b>	0.37	0.09	<b>0.91</b>
9 Botrychium	120	<b>0.76</b>	0.24	0.14	<b>0.86</b>	<b>0.52</b>	0.48
10 Pedicularis	116	0.41	<b>0.59</b>	<b>0.78</b>	0.22	0.09	<b>0.91</b>
		% > 0.5	<b>60</b>	<b>40</b>	<b>80</b>	20	<b>20</b>

Cambará, Rio Grande do Sul Highlands							
# Taxa	FR	0 to 10 kyr BP		11 to 20 kyr BP		20 to 41 kyr BP	
		$R^2_{h }$	$1-R^2_{h }$	$R^2_{h }$	$1-R^2_{h }$	$R^2_{h }$	$1-R^2_{h }$
1 Poaceae	190	<b>0.941053</b>	0.058947	<b>0.995043</b>	0.004957	<b>0.79342</b>	0.20658
2 Cyperaceae	188	<b>0.505835</b>	0.494165	<b>0.985107</b>	0.014893	<b>0.598736</b>	0.401264
3 Baccharis	188	<b>0.867134</b>	0.132866	<b>0.952809</b>	0.047191	0.431766	<b>0.568234</b>
4 Asteraceae-Tub	186	<b>0.664705</b>	0.335295	<b>0.943884</b>	0.056116	0.330651	<b>0.669349</b>
5 Melastomataceae	183	<b>0.837228</b>	0.162772	<b>0.937858</b>	0.062142	0.466385	<b>0.533616</b>
6 Eryngium	164	<b>0.783572</b>	0.216428	<b>0.99152</b>	0.00848	<b>0.694867</b>	0.305133
7 Senecio-type	160	<b>0.563002</b>	0.436998	<b>0.766707</b>	0.233293	0.45042	<b>0.54958</b>
8 Myrtaceae	159	<b>0.794556</b>	0.205444	<b>0.772857</b>	0.227143	<b>0.693159</b>	0.306841
9 Myrsine	138	<b>0.697804</b>	0.302196	<b>0.921732</b>	0.078268	0.246105	<b>0.753895</b>
10 Eriocaulon	138	<b>0.705015</b>	0.294985	<b>0.866029</b>	0.133971	0.490008	<b>0.509992</b>
11 Plantago australis-type	128	<b>0.775889</b>	0.224111	<b>0.928314</b>	0.071686	0.46934	<b>0.53066</b>
12 Araucaria angustifolia	125	<b>0.945254</b>	0.054746	<b>0.911376</b>	0.088624	0.360171	<b>0.639829</b>
13 Podocarpus	112	0.293232	<b>0.706768</b>	<b>0.865229</b>	0.134771	0.33939	<b>0.66061</b>
14 Parnassia	111	<b>0.542395</b>	0.457605	<b>0.848097</b>	0.151903	0.473687	<b>0.526313</b>
15 Celtis	109	0.20493	<b>0.79507</b>	<b>0.894</b>	0.106	0.313533	<b>0.686467</b>
16 Apiaceae	108	0.312928	<b>0.687072</b>	<b>0.806983</b>	0.193017	0.224082	<b>0.775918</b>
17 Xyris	106	<b>0.544446</b>	0.455554	<b>0.825362</b>	0.174639	0.300795	<b>0.699205</b>
18 Jungia-type	99	<b>0.527674</b>	0.472326	<b>0.788887</b>	0.211113	0.320769	<b>0.679231</b>
19 Weinmannia	96	<b>0.765332</b>	0.234668	<b>0.528129</b>	0.471871	0.322908	<b>0.677092</b>
20 Moraceae/Urticaceae	94	0.460032	<b>0.539968</b>	<b>0.902275</b>	0.097725	0.266515	<b>0.733485</b>
21 Psilate	94	0.267994	<b>0.732006</b>	<b>0.830974</b>	0.169026	0.454705	<b>0.545295</b>
Mean		<b>0.619048</b>	0.380952	<b>0.869675</b>	0.130325	0.430543	<b>0.569457</b>
% > 0.5		<b>76.19048</b>	23.80952	<b>100</b>	0	19.04762	<b>80.95238</b>
Correlation with Fr		0.570997	-0.571	0.560348	-0.56035	0.607219	-0.60722

4. Compute the first residual communality value for taxon *h* with taxon *u*:

$$S_{hhc|1} = \frac{S_{hu(1)}}{\sqrt{S_{hhs(1)}}} = \delta_{hh|u}^2,$$

and specificity  $S_{hhs(1)} = S_{hh(1)} - \delta_{hh|u}^2$ .

5. Do steps 3 and 4 recursively for each of the *p* taxa vis-a-vis taxon *h*, all taken in their natural order until all *p-1* taxa were encountered, and then sum:

$$S_{hhs} = \sum_{j=1}^p S_{hhs(j)} \quad \text{and} \quad S_{hhc} = S_{hh} - S_{hhs}.$$

6. Select the next taxon *h* and start at step 2.

How should we interpret the  $R^2_{h|}$  values? Simply stated, when  $R^2_{h|} = 1$ , then statistical redundancy is total. This im-

plies total functional integration of taxon *h* into the covariance type interaction structure of the community. When  $R^2_{h|} = 0$ , there is a total lack of redundancy, meaning that all variation in taxon *h* is specific to itself. But this also means a total lack of integration. Considering the position of the taxa on the  $0 \leq R^2_{h|} \leq 1$ , continuum, those taxa that score values nearer to 1 are deemed to exhibit trait A and those nearer to 0 are deemed to exhibit trait B.

Some interesting results are presented for two palynological spectra in Table 7. Note that meaningfulness of the results presented, and the way they are presented is a consequence of dealing with taxa whose distribution spans in good part if not totally the palynological spectrum.

Having applied the  $R^2_{h|}$  assembly trait classification rule, we now summarize the results of Table 8:

**Table 8.** Trait segregation of taxa in the Hanging Lake spectrum based on Table 7. Symbols: A – communality trait; B – specificity trait; N – trait neutral behaviour. See the main text for explanations.

#	Taxa	FR	E3	E2	E1
			0 to 10 kyr BP	11 to 20 kyr BP	20 to 41 kyr BP
1	<i>Betula</i>	133	A	A	B
2	Poaceae	133	B	A	B
3	<i>Salix</i>	132	N	N	N
4	<i>Artemisia</i>	132	A	A	B
5	Cypaeraceae	132	N	A	B
6	<i>Picea</i>	129	A	N	B
7	<i>Alnus viridis</i>	123	B	A	B
8	<i>Sphagnum</i>	121	N	A	B
9	<i>Botrychium</i>	120	A	A	N
10	<i>Pediastrum</i>	116	N	A	B

**Table 9.** Over view of the Cambará traits based on Table 7. Symbols: A – communality trait; B – specificity trait; N – trait neutral. See the explanations above.

#	Taxa	FR	E3	E2	E1
			0 to 10 kyr BP	11 to 20 kyr BP	20 to 41 kyr BP
1	Poaceae	125	A	A	A
2	Cyperaceae	112	A	A	A
3	<i>Baccharis</i>	138	A	A	B
4	Asteraceae-Tub	183	A	A	B
5	Melastomataceae	96	A	A	B
6	<i>Eryngium</i>	159	A	A	A
7	Senecio-type	109	A	A	B
8	Myrtaceae	94	A	A	A
9	Myrsine	190	A	A	B
10	<i>Eriocaulon</i>	125	A	A	B
11	<i>Plantago australis</i> -type	112	A	A	B
12	<i>Araucaria angustifolia</i>	138	A	A	B
13	<i>Podocarpus</i>	183	B	A	B
14	Pamphalea	96	A	A	B
15	<i>Celtis</i>	159	B	A	B
16	Apiaceae	109	B	A	B
17	<i>Xyris</i>	94	A	A	B
18	Jungia-type	190	A	A	B
19	<i>Weinmannia</i>	188	A	A	B
20	Moraceae/Urticaceae	188	B	A	B
21	Psilale	188	B	A	B

1. Taxa sort themselves on the communality to specificity continuum quite characteristically, depending on the epochs of the recent 40 kyr:

E1: 41 – 21 Kyr BP; cooling cycle.

E2: 20 - 11 kyr BP; warming cycle.

E3: 0 - 10 kyr BP; Holocene short-term temperature oscillations.

*Betula* in the Hanging Lake spectrum has a typically type A trait behaviour during the warming period E2 and during E3, and a highly type B trait behaviour during cold E1. Another high profile taxon that crosses the breadth of the traits is *Sphagnum*. It is quite neutral during the E3 and E2, but absolutely type B trait during E1. The lichen component *Pediastrum* is neutral during E3, displays trait A during E2 and trait B during E1. Interesting to note how *Salix* retains a trait neutral stance during all three periods with only slight byes toward a type A behaviour. On average, type A trait behaviour is dominant in the Hanging Lake spectrum during E3 and E2,

and type B behaviour during E1. Table 8 gives an over-view of traits

2. The Cambará results are summarised in Table 9. Trait B is dominant in E1 and trait A in E2. Epoch E3 is somewhat biased toward trait B, but A is still the dominant trait.

3. The shifts from B trait dominance to A trait dominance as the Late Quaternary climate begins to warm is a fact in both of the examples. Considering that the shift coincides with the shift from compositional stability to instability (see Table 7), the trait shifts take on special significance to deduce a climate related assembly rule: periods of high instability are flagged by strong interactions among the taxa (communality rule) while the opposite (the specificity rule) is characteristics for periods of high stability.

We have seen that traits can be identified that allow us to categorise taxa by their position on the continuum as community builders or individualists. It is important to note that the term “trait” emphasises a taxon’s involvement with the covariance interaction structure in the community. Pillar et al.

(2008) introduced an interesting way to reveal assembly rules by focussing on the taxon's character traits, mainly those related to functionality. On that basis, their extract assembly rules have to do with patterns of character-trait convergence (TCAP) and patterns of character-trait divergence (TCDP). Character traits are considered convergent when their distance configuration scaled up to the community-type level is highly correlated with environmental stress, also scaled up to the community type level. Pillar et al. (2008) consider character traits divergent when the distance configuration of their types (established in cluster analysis or *a priori* given) on the community type level is highly correlated with environmental stress on the community type level. These terms have their own non-linear logic that cannot be discovered easily without working through an actual example. This requires working with a good number of data matrices:

1. Matrix **B** given. This contains numerical scores for the character traits of taxa (see Orlóci and Orlóci 1985, Orlóci 1991, Pillar and Orlóci 1993). The character traits are arranged in the columns and the taxa in the rows of **B**. A characteristic cell of **B** thus contains the numerical value of the corresponding character trait in the corresponding taxon (as a population). Pillar et al. (2008) call the taxa OTUs (operational taxonomic units) following usage by Sokal and Sneath (1963, Sneath and Sokal 1975).

2. Matrix **W**. This has the taxa as its rows and community types (established in cluster analysis, if not given *a priori*) as its columns. A characteristic cell of **W** marks the presence (score 1), absence (score 0), or the quantity of the corresponding taxon in the corresponding community type.

3. Matrix **T**. This is a character traits by community types matrix derived by matrix multiplication,  $\mathbf{T}=\mathbf{B}'\mathbf{W}$ . This operation is called “up-scaling” the character traits to the community types. The latter are established in cluster analysis of the fundamental sampling units if not given *a priori*.

4. Matrix **E**. This is the usual kind of environmental data matrix. The environmental variables are arranged as the rows and community types as the columns.

5. Matrix **U**. This is derived from matrix **B**. The rows of **U** represent taxon types and its columns represent the taxa. A characteristic cell of **U** contains the value of a taxon's “belonging” to the corresponding groups of taxa. The latter are established in cluster analysis, if not given *a priori*. “Belonging” is defined here in the same sense as used by Feoli and Zuccarello (1986) and Feoli and Orlóci (1991).

6. Matrix **X**. Pillar et al. (2008) derive this by  $\mathbf{X}=\mathbf{U}'\mathbf{W}$ . In **X** the rows represent taxon types and the columns represent community types.

From the above matrices, Pillar et al. (2008) derive assembly rules via the correlations of distance matrices  $\mathbf{D}_T, \mathbf{D}_X$  with the environmental distance matrix  $\mathbf{D}_E$ . One of the assembly rules regards the intensity of the TCAP and the other the intensity of TDAP. The rule metrics are correlation coefficients:

1.  $\rho(\mathbf{TE}) = \rho(\mathbf{D}_T; \mathbf{D}_E)$  — scalar for TCAP.
2.  $\rho(\mathbf{XE}) = \rho(\mathbf{D}_X; \mathbf{D}_E)$  — an uncorrected scalar for TDAP.

What does “uncorrected” mean? If we view  $\rho(\mathbf{TE})$  as a true measure of the convergence of character traits on the ecological gradient implicit in the distance structure  $\mathbf{D}_E$ , then  $\rho(\mathbf{XE})$  will have an inference component since  $\mathbf{D}_X$  is correlated with  $\mathbf{D}_T$  and  $\mathbf{D}_T$  with  $\mathbf{D}_E$ . To see then the intensity of TDAP emerge in its true self, Pillar et al. (2008) propose the corrected metric

$$\rho(\mathbf{XE}|\mathbf{T}) = \frac{\rho(\mathbf{XE}) - \rho(\mathbf{XT})\rho(\mathbf{TE})}{[(1 - \rho(\mathbf{XT})^2)(1 - \rho(\mathbf{TE})^2)]^{1/2}} .$$

For ecological fine-points and technical explanations we refer to the original paper. In closing we pose the following question: should  $\rho(\mathbf{TE})$  not benefit from a similarly reasoned correction?

#### *Transition hotspots*

Among the compositional stability/instability indicators that we considered so far, the one with most revealing graph for detecting hotspots of compositional transitions is acceleration (Fig. 6). What can we read from the referenced acceleration graph? For one thing, we are struck by the sharp contrast between the different epochs that we labelled E1, E2, E3 in the above sections. The portion of the graph in E1 is absolutely flat (at the magnification used); this is the epoch when the climate cools and the Globe descends into the deep Ice Age. More obvious oscillations do not begin until well into the warming cycle of E2, but then dynamics becomes explosive with widely oscillating acceleration in the first half of E1. By 6 kyr BP much of the dynamics dissipated and the graph settles down into a perfectly flat segment until present. What is suggested by this characteristic pattern in the acceleration graph?

1. Intense compositional change is a delayed reaction that builds up over millennia to a maximum after sustained intense climate warming.

2. Compositional stability may not be re-established long after the extreme thermal lability is corrected.

3. The thermal drama unfolds at warming rates (Tables 2, 3) smaller than 1/9 of the warming rate of Manabe et al. (1990) prediction of 3.6 °C, that we made the basis of our comparative discussions.

#### **Synopsis: a vegetation future for the North**

An overview of the results presented in the paper suggests the likely unfolding of unusual thermal events if the predicted global 100 yr climate warming rate does in fact come in at 3.6° or higher. Taking the local thermal influx rate into account, a 3.6° rate will imply a 5.4° 100 yr rate at the northern limit of the Eastern Cool Temperate Deciduous Forest (D in Fig. 5). The predicted northward dislocation rate at this level of warming rate is 6.38° L per 100 yr. If this in

fact materialises then the thermal Northern limit of ECTDF on the Delcourt and Delcourt (1987) transect should move to the North rim of the Canadian Shield, possibly into the clay belt in the Cochrane area around 49° LN. Concurrent with this, the thermal northern limit of the Boreal-ECTDF transition belt would reach 55° LN which would leave very little room for the Boreal Forest to re-assemble as a conterminous formation. The Taiga-Tundra belt as such would disappear. The Taiga-Tundra flora would retreat to patchy refugia in the Arctic.

The effects of thermal onslaught would be seen soon, initially as forest dieback of immense geographic extent, under which a ragtag band of species, mainly those surviving the initial thermal impact, would form loose synusiae. The repopulation of the regions by the climax dominants from refugia could take centuries or possibly millennia.

The rates and consequences pointed out are clearly colossal in magnitude, but also very low probability events in the context of the known historic rates. Yet our rates are not fictitious. On this basis, they present sufficient basis for concern in the extreme, for what is at stake is nothing less than an unmitigated northern disaster. No one should hope to plan for less.

**Acknowledgements.** The author expresses thanks to M. Mihály, Forest Engineer, for her gracious help and unfailing interest in my endless projects, and to leadership of the Department of Plant Taxonomy and Ecology, ELTE, Budapest. Much of my research for this paper was completed during tenure of Visiting Professorship in the Departamento de Ecologia, Universidade Federal do Rio Grande do Sul, Brazil. I salute Prof. V. De Patta Pillar and thank him for the invaluable help.

## References

- Anderson, P.M. 1988. Late Quaternary pollen records from the Kobuk and Noatak River drainages, northwestern Alaska. *Quaternary Research* 29: 263-276.
- Anderson, R.S. 1993. A 35,000 year vegetation and climate history from Potato Lake, Mogollon Rim, Arizona. *Quaternary Research* 40: 351-359.
- Behling, H.V., De Patta Pillar, V., Orlóci, L. And Bauermann, S.G. 2004. Late Quaternary Araucaria forest, grassland (Campos), fire and climate dynamics, studied by high-resolution pollen, charcoal and multivariate analysis of the Camará do Sul core in southern Brazil. *Paleogeography, Paleoclimatology, Paleocology* 203: 277-297.
- Berry, Th. 1988. *The Dream of the Earth*. Sierra Club Books, San Francisco.
- Black, R. 2007. Bali deal: Small presents for all. BBC News, 2007/2/15, <http://news.bbc.co.uk/>.
- Bonnefille, R., Rioulet, G., Buchet, G., Icole, M., Lafont, R., Arnold, M. and Jolly, D. 1995. Glacial/Interglacial record from inter-tropical Africa, high resolution pollen and carbon data at Rusaka, Burundi. *Quaternary Science Reviews* 14: 917-936.
- Braun, E. L. 1950. *Deciduous Forests of Eastern North America*. Blakston, Toronto.
- CBC Television Fifth Estate, November 15, 2006, The Climate Denial Machine, Canada. <[www.vivelecanada.ca/article.php/20061115140323941](http://www.vivelecanada.ca/article.php/20061115140323941)>
- Colinvaux, P.A., de Oliveira, P.E., Moreno, J.E., Miller, M.C. and Bush, M.B. 1996. A long pollen record from lowland Amazonia: forest and cooling in glacial times. *Science* 274:85-88.
- Conway, T.J., Tans P.P., Waterman, L.S., Thoning, K.W., Kitzis, D.R., Masarie, K.A. and N. Zhang. 1994. Evidence of interannual variability of the carbon cycle from the NOAA/CMDL global air sampling network. *J. Geophys. Research* 99: 22831-22855.
- Cruikshank, D.P. 1986. *Mauna Kea*. A guide to the upper slopes and observatories. University of Hawaii at Manoa, Institute of Astronomy, Honolulu, Hawaii, U.S.A.
- Cwynar, L. C. 1982. A Late-Quaternary vegetation history from Hanging Lake, northern Yukon. *Ecol. Monog.* 52:,1-24.
- Delcourt, P.A. and Delcourt, H.R. 1987. *Long-term Forest Dynamics of the Temperate Zone*. Ecological Studies 63, Springer, New York.
- Ege, E. and Christiansen, J.L. (eds.). 2002. *Sceptical Questions and Sustainable Answers*. The Danish Ecological Council, Copenhagen. ISBN: 87-89843-37-1. <[www.ecocouncil.dk/download/sceptical.pdf](http://www.ecocouncil.dk/download/sceptical.pdf)>
- Feoli, E. and Orlóci, L. 1991. Fuzzy components in community level comparisons. In: E. Feoli and L. Orlóci (eds.), *Computer Assisted Vegetation Analysis*, Kluwer, London, pp. 87-93.
- Feoli, E. and Zuccarello, V. 1989. Syntaxonomy: a source for useful fuzzy sets for environmental analysis? *Coenoses* 3: 141-147.
- Global Pollen Database. 2007. Address: <[www.ncdc.noaa.gov/paleo/pollen.html](http://www.ncdc.noaa.gov/paleo/pollen.html)>
- Gore, A. 1992. *Earth in the Balance. Ecology and the Human Spirit* Houghton Mifflin, Boston.
- Gore, A. 2006. An Inconvenient truth. Paramount Classics and Participant Productions, David Gugenheimer directing. Hollywood, CF.
- Grady, R.E. 2001. Search for the "Son of Kyoto". *Time*, June 25, p. 17.
- Gray, J. and Se, J.S. 1984. Climatic implications of the natural variation of D/H ratio in tree ring cellulose. *Earth Planet Sc. Lett.* 70: 129-138.
- IPCC — Intergovernmental Panel on Climate Change. 2001. Third Assessment Report. – Climate Change. Web address: <<http://www.ipcc.ch>>
- IPCC — Intergovernmental Panel on Climate Change. 2007. Fourth Assessment Report – Climate change. <[www.ipcc.ch](http://www.ipcc.ch)>
- Jacobs, B.F. 1985. A middle Wisconsin pollen record from Hay Lake, Arizona. *Quaternary Research* 24: 121-130.
- Keeling, C.D., Bacastow, R.B., Bainbridge, A.E., Ekdahl, C.A., Guenther, P.R. and Waterman, L.S. 1976. Atmospheric carbon dioxide variations at Mauna Loa Observatory, Hawaii. *Tellus* 28: 538-551.
- Kershaw, A.P. 1994. Pleistocene vegetation of the humid tropics of northeastern Queensland, Australia. *Palaeogeography, Palaeoclimatology, and Palaeoecology* 109: 399-412.
- Kluger, J. 2001. A climate of despair. *Time* April 9, pp. 30-36.
- Krajina, V. J. 1963. Biogeoclimatic biomes on the Hawaiian Islands. *Newsletter of the Hawaiian Botanical Society* 7: 93-98.
- Küchler, A.W. 1974. *Vegetation Mapping*. Ronald Press, New York.

- Küchler, A.W. 1990. Natural Vegetation. In: Espenchade Jr., E.B. and Morrison, J.L. (Eds.) *Rand McNally Good's World Atlas*, 18th edn. Rand McNally, New York, pp. 8-9.
- Lemonic, M.D. 2001. Life in the greenhouse. Making a case that our climate is changing. *Time*, April 9, pp. 24-29.
- Lomborg, B. 2001a. The truth about the environment. *The Economist*, August 4-10, pp. 63-65.
- Lomborg, B. 2001b. *The Skeptical Environmentalist: Measuring the Real State of the World*, Cambridge University Press, Cambridge.
- Lozhkin, A.V., Anderson, P.M., Eisner, W.R., Ravako, L.G., Hopkins, D.M., Brubaker, L.B., Colinvaux, P.A., Miller, M.C. 1993. Late Quaternary lacustrine pollen records from southwestern Beringia. *Quaternary Research* 39: 314-324.
- Manabe, S., Bryan, K. and Spelman, M. J. 1990. Transient response of a global ocean-atmosphere model to a doubling of atmospheric carbon dioxide. *J. Phys. Oceanogr.* 20: 722-749.
- Mason, J. 1990. The greenhouse effect and global warming. Information Office, British Coal, C.R.E. Stoke Orchard, Cheltenham, Gloucestershire, U.K. GL52 4RZ.
- Milankovitch, M.M. 1941. Canon of isolation and the Ice-Age problem. *Royal Serb Acad. Spec. Publ.* 133.
- NSF - National Research Council. 2001. Climate Change Science: An Analysis of Some Key Questions. Washington, USA. Find abstract in "Global Change Digest: May/June 2001 Edition". <[www.globalchange.org/gccd/Digest/homepage.html](http://www.globalchange.org/gccd/Digest/homepage.html)>
- Orlóci, L. 1975. Measurement of redundancy in species collections. *Vegetatio* 31: 65-67.
- Orlóci, L. 1978. *Multivariate Analysis in Vegetation research*. 2nd ed. W. Junk, The Hague.
- Orlóci, L. 1991. On character-based plant community analysis: choice, arrangement, comparison. *Coenoses* 6: 103-107
- Orlóci, L. 1994. Global warming: the process and its anticipated phytoclimatic effects in temperate and cold zones. *Coenoses* 9: 69-74. — Pre-publication version <<http://publish.uwo.ca/~lorloci/Files.html>>
- Orlóci, L. 2001. Prospects and expectations: reflections on a science in change. *Community Ecology* 2: 187-196.
- Orlóci, L. 2008. Trajectory analysis: powerful conceptual tool for understanding nature. <<http://vegetationdynamics.blogspot.com/>> and links "Featured paper", "Appendices".
- Orlóci, L. and Orlóci, M. 1985. Comparison of communities without the use of species: model and example. *Ann. Bot. (Roma)* 43: 275-285.
- Orlóci, L. and Orlóci, M. 1995. *Sampling and Data Analysis. Theory, problems, examples*. Scada Associates, London, Canada. Mimeographed.
- Orlóci, L., Pillar, V. D., Anand, M. and Behling, H. 2002. Some interesting characteristics of the vegetation process. *Community Ecology* 3: 125-146.
- Orlóci, L., Pillar, V.D., and Anand, M. 2006. Multiscale analysis of palynological records: new possibilities. *Community Ecology* 7: 53-68.
- Parnesan, C. 2006. Ecological and evolutionary responses to recent climate change. *Annual Review of Ecology, Evolution, and Systematics* 37: 637-639.
- Petit, J.R., Jouzel, D. Raynaud, D., Barkov, N.I, Barnola, J.M., Basile, I., Bender, M., Chappellaz, J., Davis, J., Delaygue, G., Delmotte, M., Kotlyakov, V.M., Legrand, M., Lipenkov, V., Lorius, C., Pepin, L., Ritz, C., Saltzman, E. and Stievenard, M. 1999. Climate and atmospheric history of the past 420,000 years from the Vostok Ice Core, Antarctica. *Nature* 300: 429-436
- Petit, J.R., Jouzel, J. Raynaud, D., Barkov, N.I, Barnola, J.M., Basile, I., Bender, M., Chappellaz, J., Davis, J., Delaygue, G., Delmotte, M., Kotlyakov, V.M., Legrand, M., Lipenkov, V., Lorius, C., Pepin, L., Ritz, C., Saltzman, E. and Stievenard, M. 2001. Vostok Ice Core Data for 420,000 years, IGBP PAGES/World Data Center for Paleoclimatology Data Contribution Series #2001-076. NOAA/NGDC Paleoclimatology Program, Boulder CO, USA.
- Pillar, V., Duarte, L.S., Sosinski, E.E. and Joner, F. 2008. Sorting out trait-convergence and trait-divergence assembly patterns in ecological community gradients. *J. Veg. Sci.* (In press.)
- Pillar, V.D., Orlóci, L. 1993. *Character-based Vegetation Analysis: the Theory and an Application Program*. Ecological Computations Series (ECS): Vol. 5. SPB Academic Publishing bv, The Hague, The Netherlands.
- Schweingruber, F.H. 1996. *Tree Rings and Environment Dendroecology*. Paul Haupt, Stuttgart.
- Singh, G. and Geissler, E.A. 1985. Late Cainozoic history of vegetation, fire, lake levels and climate at Lake George, New South Wales, Australia. *Philosophical Transactions of the Royal Society of London Series B*, 311:379-447.
- Sneath, P.H.A. and Sokal, R.R. 1973. *Numerical Taxonomy. The Principles and Techniques of Numerical Classification*. Freeman, San Francisco.
- Sokal, R.R. and Sneath, P.H.A. 1963. *Principles of Numerical taxonomy*. Freeman, San Francisco.
- Tans, P. 2008. NOAA/ESRL records on CO<sub>2</sub> in Mauna Loa's atmosphere. <[www.esrl.noaa.gov/gmd/ccgg/trends](http://www.esrl.noaa.gov/gmd/ccgg/trends)>.
- Thoning, K.W., Tans, P.P. and Komhyr, W.D. 1989. Atmospheric carbon dioxide at Mauna Loa Observatory 2. Analysis of the NOAA GMCC data, 1974-1985. *J. Geophys. Research* 94: 8549-8565.
- Trewartha, G.T. 1990. Climatic Regions. In: Espenchade, E.B. Jr. and Morrison, J.L. (Eds.), *Rand McNally Good's World Atlas*, 18th ed. Rand McNally, New York, pp. 8-9.
- Trewartha, G.T. 2001. Global Mechanism of UNCCD, Via del Serafico 107, 00142 Rome, Italy. Web address: [www.gm-uncd.org/English/Field/aridity.htm](http://www.gm-uncd.org/English/Field/aridity.htm).
- Walter, H., Harnickell, E. and Mueller-Dombois, D. 1975. *Climate Diagram Maps*. Springer, New York.
- Watts, W.A., Bradbury, J.P. 1982. Paleocological studies at Lake Patzcuaro on the west-central Mexican Plateau and at Chalco in the Basin of Mexico. *Quaternary Research* 17: 56-70.
- Watts, W.A., Hansen, B.C.S. and Grimm, E.C. 1992. Camel Lake: A 40,000-yr record of vegetational and forest history from northwest Florida. *Ecology* 73: 1056-1066.
- Wilkins, G.R., Delcourt, P.A., Delcourt, H.R., Harrison, F.W. and Turner, M.R. 1991. Paleocology of central Kentucky since the last glacial maximum. *Quaternary Research* 36:224-239.
- World Data Center for Paleoclimatology. 2002. Address: <[www.ngdc.noaa.gov/paleo/icecore/antarctica/vostok](http://www.ngdc.noaa.gov/paleo/icecore/antarctica/vostok)>

Received April 22, 2008  
 Revised May 20, 2008  
 Accepted June 5, 2008